Archives of Civil and Mechanical Engineering (2024) 24:169
https://doi.org/10.1007/s43452-024-00979-6

ORIGINAL ARTICLE

Sub-global equilibrium method for identification of elastic parameters based on digital image correlation results

Marcin Nowak[1] · **Paweł Szeptyński**[2] · **Sandra Musiał**[1] · **Michał Maj**[1]

Received: 15 November 2023 / Revised: 13 May 2024 / Accepted: 19 May 2024

Abstract
In this work, a new, simple method is presented, which enables identification of material properties of solids basing on the digital image correlation (DIC) measurements. It may be considered as a simplified alternative of low computational complexity for the well-known finite element model updating (FEMU) method and virtual fields method (VFM). The idea of the introduced sub-global equilibrium (SGE) method is to utilize the fundamental concept and definition of internal forces and its equilibrium with appropriate set of external forces. This makes the method universal for the use in the description of a great variety of continua. The objective function is the measure of imbalance, namely the sum of squares of residua of equilibrium equations of external forces and internal forces determined for finite-sized part of the sample. It is then minimized with the use of the Nelder–Mead downhill simplex algorithm. The efficiency of the proposed SGE method is shown for two types of materials: 310 S austenitic steel and carbon-fiber-reinforced polymer (CFRP). The proposed method was also verified based on FE analysis showing error estimation.

Keywords Identification of material constant · Digital image correlation · Nelder–Mead downhill simplex algorithm · Finite element analysis · Optimization · Linear elasticity

1 Introduction

The appropriate determination of the material parameters of the constitutive models is one of the crucial factors that influence the final results of any numerical simulation. The classic methods of measuring these parameters (such as Young's modulus, Poisson's ratio, initial yield stress, Lankford's coefficient—plastic strain ratio) require the careful preparation of sample geometry, since any imperfection may flaw the results of the performed tests [1]. Furthermore, during material testing, the deformation must be uniform throughout the gauge section to make use of the notions of nominal stress (stress averaged over the sample's cross section) or relative elongation (strain averaged along the gauge length). In the absence of homogeneous deformation, for example, when the onset of localization occurs, these methods are not suitable for determining materials parameters. Any imperfection or heterogeneity of the sample as well as the alignment of the testing machine–sample setup can additionally introduce errors that are difficult to estimate.

With the development of new measuring techniques for material testing, such as digital image correlation (DIC) [2] or electronic speckle pattern interferometry (ESPI) [3], new possibilities for the identification of material constants arise which do not have the disadvantages mentioned above [4, 5]. One group of these techniques is based on solving the inverse problem. The use of the finite element model updating method (FEMU) allows the characterization of very complex constitutive relations. The main idea behind this method is to use an over-determined deformation measurement for iterative updating of the FE constitutive model [6].

✉ Michał Maj
mimaj@ippt.pan.pl

Marcin Nowak
nowakm@ippt.pan.pl

Paweł Szeptyński
pszeptynski@pk.edu.pl

Sandra Musiał
smusial@ippt.pan.pl

[1] Institute of Fundamental Technological Research, Polish Academy of Sciences, Pawińskiego 5B, 02-106 Warsaw, Poland

[2] Division of Structural Mechanics and Material Mechanics, Faculty of Civil Engineering, Cracow University of Technology, Kraków, Poland

Published online: 06 June 2024

In the standard FEMU method, the discrepancy between the measured displacement field and the one computed in FEA with the use of a postulated constitutive relation is minimized [7]. In another work [8], the calibration procedure of parameters for a concrete constitutive model using DIC and inverse analysis was investigated. The difference between the experimental and numerical displacement field was used for discrepancy minimization. In a similar way, the authors of [9] described a general framework which couples the DIC method with the finite element analysis to estimated materials parameters. It is not only the difference between the experimentally determined and the computed displacement field that is minimized, the external load is also taken into consideration. In a similar way, another research [10] compares the experimentally measured force applied to the sample with the resultant force from the several cross sections computed from the stress field obtained on the basis of the DIC results.

An alternative approach is to minimize so-called "equilibrium gap" (EG), namely an Euclidean norm of unbalanced forces determined with the use of postulated constitutive relation and measured displacement field [11]. Modified EG approaches have also been introduced, namely constitutive law error (CLE) concept in which an energy- measure of unbalanced forces in minimized [12] or reconditioned equilibrium gap (REG) method, which makes the original GE much less sensitive to noise [13].

The full-field displacement field can be also obtained by moiré interferometry. In [14], the Bayesian identification of elastic constants in multi-directional laminate was performed. In analysis, an open hole plate was used to create complex displacement fields that are strongly influenced by all the elastic constants. Authors found that the confidence levels associated with the identification of the four orthotropic elastic constants were not uniform.

Recently, the virtual field method (VFM) has also gained popularity [15, 16] which utilizes the principle of virtual work. This method requires postulating kinematically admissible displacement fields which can be sometimes significant challenge especially when dealing with non-linear constitutive models [17]. The versatility of this method has led to its widespread adoption across various applications, giving rise to numerous specialized tools. One such example is available at www.matchid.eu. There are several works in which the VFM has been successfully applied to identify the material parameters of the assumed constitutive relations based on DIC measurements. The elastic materials parameters for unidirectional carbon-fiber-reinforced polymer (CFRP) sheets treated as orthotropic linear elastic solid has been identified [18]. In the work [19], the authors identified the constitutive parameters and damage evolution parameters in an elastic–plastic model corresponding with von Mises yield condition with isotropic hardening and Lemaitre's elastic–plastic damage coupling. In [20], a technique has been introduced to effectively determine the anisotropic plasticity constitutive parameters for sheet metals subjected to high strain rates. This is achieved by analyzing the inertial acceleration, as well as the strain and strain rate field data from the impact test, utilizing the dynamic version of the virtual field method

Not only DIC method can be used to measure a displacement field in VFM. In [21], the grid method has been successfully applied to identify a non-linear model for composites. In [22], the authors examined the problem of influence of random noise on the uncertainty of the elastic constants estimated via the VFM. Authors derived criteria, according to which the special virtual fields could be optimized in the sense, that the fields corresponding with minimal value of sensitivity-to-noise coefficient provide the most accurate results. Finally, in [23], an optimal procedure for the identification of material's parameters from experimentally measured displacement field is proposed. The primary objective of this paper is to enhance the existing optimality aspect by examining all the aforementioned identification methods regarding their responsiveness to measurement uncertainties. Similarly in [24], the general framework for identification of constitutive parameters is postulated. The sensitivity of several approaches available in the literature to a white noise in the data is evaluated and compared. Recently, the VFM has been used to reconstruct the heterogeneity distribution of solid materials [25]. The presented results of the reconstruction have shown that the suggested VFM methods can successfully recover inclusions despite the presence of minimal noise.

The goal of this work is to propose the new method which can be an alternative to the above-mentioned methods. In the proposed approach, an equilibrium between external loads and stresses integrated along an imaginary cut-surface is considered. Therefore, the method was named the Sub-Global Equilibrium method. The idea is that as the stresses are calculated with the use of estimated material parameters, the optimal choice of those parameters minimizes the residuum of the equilibrium equation. The details are presented in the following chapter.

The proposed methodology may prove to be useful, especially in the description of composite materials. The practical need for finding the mechanical characteristics of a simplified model of homogeneous material, which is equivalent to the considered composite (inhomogeneous) material with respect to chosen criteria, has led to the development of various homogenization methods, starting from early concepts of the rule of mixtures [26, 27] and finishing with various methods of numerical homogenization based on the analysis of a representative volume element (RVE) or a

representative unit cell (RUC); brief summaries of classical results may be found in the literature [28, 29].

The proposed method of the identification of material parameters enables homogenization based directly on extensive experimental data—namely, a high-resolution discrete displacement field determined by the DIC method in the whole region of interest of an examined composite material—and on the choice of a mathematical constitutive model of homogenized material. This approach is free from defining the RVE and assuming interactions between neighboring RVEs. Parameters of the assumed physical model are found based directly on the experimental results in the process of optimization, which minimizes the error in satisfying the equilibrium conditions. This method may also be easily automatized as an extension of the DIC postprocessing software as it does not require any FEM calculations.

The following features of the proposed method are the most worth mentioning:

- The proposed sub-global equilibrium (SGE) method is built upon the most fundamental concepts of continuum mechanics, namely the notion of internal force and an idea of its equilibrium with an appropriate system of external loads. As a result, the method is not restricted to any particular theory such as linear or non-linear elasticity or plasticity nor is it constrained by, e.g., assumptions respective for the principle of virtual works. It may be as well utilized within any of the theories of generalized continua.
- The only input required for the method is the DIC full-field displacement measurement. It does not require iteratively updated FEA results as it is needed when using the FEMU approach and it also does not need determining the virtual fields as in the case of the VFM.
- The method optimizes the estimates of the material constants with the use of the Nelder–Mead algorithm, which is an efficient tool in solving non-linear problems. Additionally, it does not require any computation of gradients and thus it deals also with non-smooth problems.
- While the validation of the method is presented here in the context of linear elasticity, the method may be easily generalized for the case of non-linear problems—the details are provided in the summary and conclusions section.

2 Physical motivation for the proposed methodology

Concerning the problem of the identification of material mechanical properties, it is in fact the problem of finding a mathematical relationship between a measure of strain (derived from observed displacements according to the assumed kinematic relations) and a measure of stress. The proposed methodology is restricted to problems in which the general form of such a constitutive relation is assumed in advance and only numerical values of parameters appearing in these relations need to be found.

Let us consider the mathematical formulation of a general problem of the theory of elasticity. We will consider the distribution of displacement vector field as a given experimental data—in the presented methodology, it is a known discrete set of components of the displacement vector obtained via DIC analysis is considered. Once displacement is known, the distribution of any strain measure field may be computed according to appropriate geometric (kinematic) relations. In this sense, geometric relations are identically satisfied as they serve as a definition for calculating the strain. Additionally, the unknown constitutive relations must be identically satisfied by assumption—they provide us with explicit formulae for calculating stress with the use of determined strains. With this in mind, we may notice that among all governing equations of a general problem of non-linear elasticity, these are only the equilibrium equations that may not be satisfied for a given displacement field and an estimated constitutive relation. This observation leads to the conclusion that residua of equilibrium equations written down for the stress field determined according to an estimated constitutive relation may serve as a measure of the discrepancy between the actual and estimated mechanical characteristics of the considered material.

2.1 Local and global equilibrium

For the purpose of simplicity, we shall consider only quasi-static loading processes. The proposed approach for validation of the investigated constitutive relation may concern both local (in point) equilibrium governed by equilibrium equations

$$\sigma_{ij,j} + b_i = 0, \quad i = 1, 2, 3 \tag{1}$$

as well as global equilibrium, which requires that the vector sum of all forces and the moment of those forces about any point must be by definition of the equilibrium—zero vectors.

$$\left(\sum \mathbf{F} = \mathbf{0}\right) \wedge \left(\forall_P \sum \mathbf{M}_P = \mathbf{0}\right). \tag{2}$$

Concerning the latter notion of equilibrium, it is obvious that a sample tested in a machine is in global equilibrium. We may conclude, however, that if a body is in global equilibrium, then any part of that body—cut out with the use of imaginary surfaces—must also be in equilibrium. This is how the notion of internal forces is introduced in continuum mechanics (Fig. 1). The discussed equilibrium requires that the system consisting of external forces applied to that part

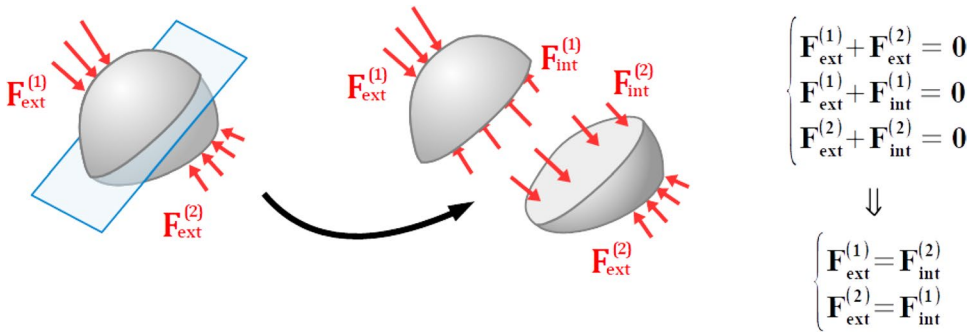

Fig. 1 Static equivalence of a system of external forces applied to one part of a body and a system of internal forces applied to the remaining part of the body

and internal forces (integrated stresses) corresponding with the considered cut-surface must be in global equilibrium. We shall use the term "sub-global" equilibrium to describe such a situation.

Both approaches—the local approach, and the sub-global approach—may be used to identify the mechanical properties of a material. Another approach is to make use of the equivalent global formulation which is the weak formulation of local equilibrium equations, namely so-called variational principles of elasticity—this is in fact the idea behind the VFM, which is not the subject of this research. The local approach requires the equilibrium equations (1) to be satisfied identically in all points; if it is so, the investigated constitutive relation is a true one. Concerning the DIC methods, this would mean that the appropriate equilibrium equation must be satisfied in each point in which stress is determined, which would lead to a relatively large and strongly over-determined system of equations if all those equations are to be satisfied simultaneously. One may consider the residuum in each point as a measure of discrepancy between the true and supposed characteristics of material mechanical properties.

The sub-global equilibrium (SGE) may be treated in a similar manner. We may consider a certain imaginary cut-surface π and determine internal tractions according to the assumed constitutive relation. These tractions may be then integrated and the resultant forces and torques should satisfy the SGE equation. The greater the number of equilibrium conditions, the more reliable the proposed approach—two such conditions may be stated, e.g., for uniaxial tensile test with hinged clamps (axial force and moment equilibrium) or for biaxial tests (two force equilibrium conditions). We restrict, however, our considerations here to only simple cases, which may be realized with the use of standard testing machines. We shall deal only with samples loaded axially. The measured force F_{exp} applied to the specimen and integrated internal forces F_π corresponding with profile π and calculated according to the supposed constitutive relation should satisfy the SGE equation:

$$F_{\text{exp}} - F_\pi = 0. \tag{3}$$

A measure g of the discrepancy between the true and supposed constitutive relation may be defined as a square of a residuum of that equation:

$$g = R^2 = (F_{\text{exp}} - F_\pi)^2, \tag{4}$$

where R is a residuum of the sub-global equilibrium equation corresponding with profile π. It is obvious that it is not only the assumed constitutive relation that influences the magnitude of residuum, the choice of position and geometry of profile π also does. For this reason, it is suggested in the proposed methodology to perform the identification of mechanical properties of material, based on a greater number I of different tested specimens and considering a finite but large number K of distinct cut-surfaces π_k (profiles) and calculating the residua of sub-global equilibrium conditions. The measure of deviation of the supposed constitutive relation from the true physical characteristics may be simply a sum of squares of residua $R_{i,k}$ calculated for all tested samples and all considered profiles:

$$g = \sum_{i=1}^{I}\sum_{k=1}^{K}(R^{(i,k)})^2 = \sum_{i=1}^{I}\sum_{k=1}^{K}\left(F_{\text{exp}}^{(i)} - F_\pi^{(i,k)}\right)^2. \tag{5}$$

The fact that measure g makes an account for multiple sample geometries as well as for distinct load cases results in the fact that the proposed methodology may provide estimates of material constants which are not influenced by a specific and arbitrary chosen type of sample or type of test. Such a summation, however, may introduce an error, due to fact that each residuum is influenced by different imperfections in preparation of the sample and of the experimental setup as well as inaccuracies in realization of the test. As a result, the magnitudes of these residua may be significantly affected solely by these geometrical factors. This difficulty may be at least partially overcome by the use of appropriate weights accounting for these imperfections (see Eq. (23)).

It is also important to notice, that only I experiments need to be performed since all K residua may be calculated using only a single ith DIC measurement.

3 Description of a general algorithm

The proposed methodology in the presented variant is restricted to the identification of constant parameters of an a priori assumed form of the constitutive relation rather than finding a functional relationship between components of assumed tensorial measures of stress and strain. The following general form of the constitutive relation is considered:

$$\mathbf{S} = f(p_1, p_2, ..., p_N, \mathbf{E}), \tag{6}$$

where $\mathbf{S}$ and $\mathbf{E}$ stand for a certain stress tensor and a certain strain tensor, respectively; function f is known and parameters p_n $(n = 1, ..., N)$ are constants. For the sake of simplicity, we shall narrow our considerations to only linear elastic solids in plane stress state, for which $\mathbf{S} = \boldsymbol{\sigma}$ is the Cauchy stress tensor while $\mathbf{E} = \boldsymbol{\varepsilon}$ is the Cauchy small strain tensor. Constant parameters p_n may be considered equal to the components of the stiffness tensor S_{ijkl}, which satisfy the generalized Hooke's Law:

$$\sigma_{ij} = S_{ijkl}\varepsilon_{kl}. \tag{7}$$

In fact, slightly different parameters will be chosen. Natural generalization of the proposed methodology for the cases of non-linear problems is discussed in the conclusions section.

Once the choice of stress and strain measure is made and the general form of the constitutive relation is assumed, it is possible to formally state an optimization problem. The formal structure of the optimization task is as follows:

- Let $\mathcal{P} \in \mathbb{R}^N$ be a region of admissible values of material parameters $p_1, p_2, ..., p_N$. Let us denote $\mathbf{p} = (p_1, p_2, ..., p_N) \in \mathcal{P}$.
- Let $g(\mathbf{p})$ be the objective function, namely the sum of the residua of sub-global equilibrium equations written down for all considered profiles:

$$g = \sum_{i=1}^{I} \sum_{k=1}^{K} \left(F_{\text{exp}}^{(i)} - F_{\pi}^{(i,k)} \right)^2. \tag{8}$$

- Minimize $g(\mathbf{p})$ with respect to $\mathbf{p} \in \mathcal{P}$,
  - subject to constraint $\mathbf{h}(\mathbf{p}) \geq 0$.

The system of inequality constraints $\mathbf{h}(\mathbf{p}) \geq 0$ ensures the positive-definiteness of elasticity tensors, which is required by the second law of thermodynamics (see Eq. (12)). Specific form of these constraints depends on the choice of parameters $(p_1, p_2, ..., p_N)$. Each of the above statements will be discussed below.

3.1 Control variables

Because the two-dimensional linear elasticity problem is considered, the mechanical properties of a solid may be characterized by at most six independent components of a fully anisotropic plane elasticity tensor. However, because the internal structure of materials which have been investigated exhibits at least single planar symmetry, the problem may be simplified so that only four components are considered independent:

$$N = 4 \;\Rightarrow\; \mathbf{p} = (p_1, p_2, p_3, p_4). \tag{9}$$

An appropriate alignment of the orientation of the microstructure of the samples (i.e., orientation of the principal axes of orthotropy) enables description of the material with the use of an orthotropic plane elasticity tensor of the following form:

$$\mathbf{S} = \begin{bmatrix} S_{1111} & S_{1122} & 0 \\ S_{1122} & S_{2222} & 0 \\ 0 & 0 & 2S_{1212} \end{bmatrix}. \tag{10}$$

Such a form of a plane orthotropic tensor only corresponds to such coordinate systems for which the axes are aligned with the planes of symmetry of the material. Control variables are defined as scaling parameters relating the estimated values of components of the stiffness tensor to the reference values S_{ijkl}^{ref} in the following way:

$$S_{1111} = p_1 S_{1111}^{\text{ref}},\; S_{1122} = p_2 S_{1122}^{\text{ref}}, ...$$

while the values S_{ijkl}^{ref} themselves are simultaneously the initial guess values for the iterative optimization algorithm. These are the components of an isotropic stiffness tensor

$$\mathbf{S} = \begin{bmatrix} S_{1111}^{\text{ref}} & S_{1122}^{\text{ref}} & 0 \\ S_{1122}^{\text{ref}} & S_{1111}^{\text{ref}} & 0 \\ 0 & 0 & S_{1111}^{\text{ref}} - S_{1122}^{\text{ref}} \end{bmatrix}, \tag{11}$$

which is roughly approximated in the following way: a single standard uniaxial tension test enables finding an approximate value of the Young's modulus while the value of Poisson's ratio is assumed to be in the interval of thermodynamically admissible values $(-1;0.5)$. It is important to underline that the assumption of isotropy has nothing in common with the true internal symmetries of the material structure and is chosen only for the sake of the simplicity of the determination of the guessed values in the initial step of the optimization algorithm. The anisotropy of the investigated stiffness tensor emerges automatically in the process of optimization.

3.2 Thermodynamical constraint and admissible values of control variables

In the subsequent iteration steps, new values of components of the stiffness tensor are determined; however, not all of them are considered admissible due to the thermodynamical constraints imposed on elastic constants. To satisfy the second law of thermodynamics it is required for the stiffness tensor to be a positive-definite tensor, namely that all of its eigenvalues (termed the Kelvin moduli) are positive [30]. For a general plane orthotropic tensor given by Eq. (10), this requires that:

$$\begin{aligned} &(S_{1111}+S_{2222})+\sqrt{(S_{1111}-S_{2222})+4S_{1122}^2}>0,\\ &(S_{1111}+S_{2222})-\sqrt{(S_{1111}-S_{2222})+4S_{1122}^2}>0,\\ &S_{1212}>0. \end{aligned} \tag{12}$$

3.3 Objective function

The objective function, i.e., the sum of squares of residua of sub-equilibrium equations, is evaluated for a given set of experimental data and current estimates of values of material parameters.

3.3.1 Flowchart of the algorithm

In the flowchart presented below, the indices $i = 1, 2, ..., I$ and $k = 1, 2, ..., K$ correspond to ith sample and kth profile, respectively. Because only small strains (linear elasticity) are considered, the difference between the reference and actual configuration of a body has a minor influence on the described procedure and may be disregarded. In the following description, coordinates $\mathbf{x}$ denote the position in the reference configuration.

1. Consider the ith sample.
2. Perform the measurement of the magnitude of external load $F_{\text{exp}}^{(i)}$ and DIC measurement of the displacement field $\mathbf{u}^{(i)}(\mathbf{x})$.
3. Determine the Cauchy small strain tensor field $\boldsymbol{\varepsilon}^{(i)}(\mathbf{x})$.
4. Define the set of profiles π_k that intersect the sample. The profiles are in fact polygon lines, the segments of which are all of length Δs.
5. Determine the outward unit vector $\mathbf{n}^{(i,k)}(\mathbf{x})$ perpendicular to the profile for each segment of the profile π_k.
6. For each segment of profile π_k, calculate the corresponding Cauchy small strain tensor $\tilde{\boldsymbol{\varepsilon}}^{(i,k)}$—it is obtained as the arithmetic mean of strains belonging to the neighborhood of the center of the considered segment of radius $\frac{\Delta s}{2}$, (Fig. 2).

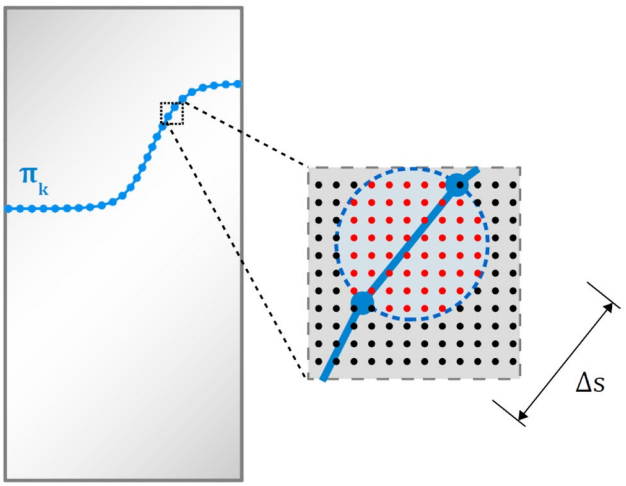

Fig. 2 Set of points taken into account when computing the stress tensor for a segment of a profile

7. For each segment of profile π_k, calculate the corresponding stress tensor $\boldsymbol{\sigma}^{(i,k)}$ according to the relation

$$\boldsymbol{\sigma}^{(i,k)} = \mathbf{S}\cdot\tilde{\boldsymbol{\varepsilon}}^{(i,k)}. \tag{13}$$

8. Determine the stress vectors (internal tractions vector) according to the Cauchy stress theorem:

$$\mathbf{t}^{(i,k)}(\mathbf{x}) = \boldsymbol{\sigma}^{(i,k)}(\mathbf{x})\cdot\mathbf{n}^{(i,k)}(\mathbf{x}),\quad \mathbf{x}\in\pi_k. \tag{14}$$

9. Project the stress vector in all points of each profile onto the direction of external loading force given by unit vector $\mathbf{m}$ and integrate stresses to obtain the sum of the system of internal forces (Fig. 3):

$$F_{\pi}^{(i,k)} = \iint_{\pi_k}\left[\mathbf{t}^{(i,k)}(\mathbf{x})\cdot\mathbf{m}\right]\mathrm{d}a. \tag{15}$$

10. Repeat steps 5–9 for all K profiles.
11. Repeat steps 1–9 for all I samples.
12. Calculate the value of the objective function which is the sum of squares of the residua of sub-global equilibrium condition:

$$g(\mathbf{p}^{(n)}) = \sum_{i=1}^{I}\sum_{k=1}^{K}\left(F_{\text{exp}}^{(i)} - F_{\pi}^{(i,k)}\right)^2, \tag{16}$$

where vector $\mathbf{p}^{(n)}$ contains the current estimate of elastic material parameters.

The above algorithm was written for a continuum. DIC gives us discrete set of data for which the processing requires a numerical approach. The procedure described in Sect. 3.3.1 has been implement in Python programming

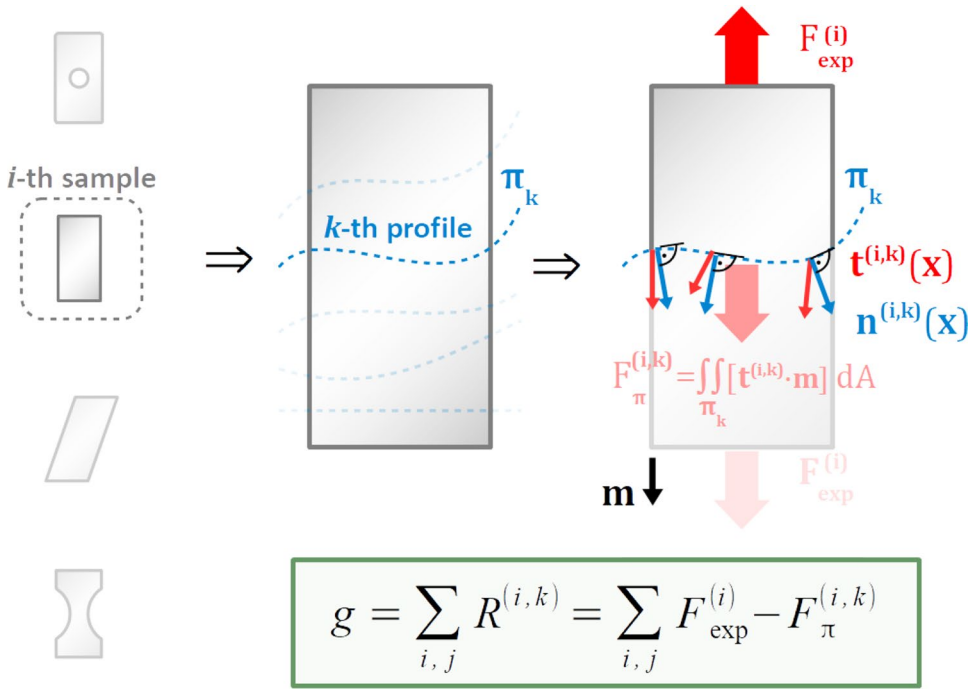

Fig. 3 Evaluation of the objective function

language as the extension module for the ThermoCorr program [31]. The Nelder–Mead downhill simplex method was implemented according to previous work [32].

3.4 Optimization subroutine

The considered optimization task is a common problem of the minimization of the residual sum of squares (RSS). Multiple algorithms for solving such problems are known. In this article, the optimization task is solved with the use of the Nelder–Mead downhill simplex method, commonly referred to as the "amoeba method" [33]. The optimization is performed in an N-dimensional space of admissible values of control parameters $\mathcal{P} \in \mathbb{R}^N$. At the beginning of the optimization process, $(N+1)$ sets of initial guess values are assumed as $\mathbf{p}^{(q)} = \left(p_1^{(q)}, p_2^{(q)}, ..., p_N^{(q)}\right)$, $(q = 1, ..., N+1)$. These sets correspond with the $(N+1)$ coordinates of vertices of an N-dimensional simplex in $\mathcal{P}$, which is the generalization of the simplest possible polyhedron for N dimensions.

The value of the objective function is then calculated for each of those sets $g(\mathbf{p}^{(q)})$ $(q = 1, ..., N+1)$ and the obtained values are arranged in increasing order, so that the last set provides the worst estimate. The centroid is then calculated for all but the last vertices. In the following steps, the simplex is transformed in such a way that the vertex corresponding with the worst try is reflected about the centroid, its distance from the centroid is expanded or contracted or the whole simplex is shrunk. The procedure is repeated until one of the criteria given in Eq. (17) is satisfied. In the presented implementation of the Nelder–Mead method, the algorithm is terminated if either the number of iterations *maxiter* exceeds 200 or the absolute value of difference of estimates of unknown parameters at the nth and $(n+1)$st iteration will be less than 0.001:

$$(maxiter > 200) \ \vee \ \left(|p^{(n)} - p^{(n+1)}| < 0.001\right). \tag{17}$$

The downhill simplex optimization algorithm proves to be very sensitive to initial guess values, which should be chosen with care. The Nelder–Mead method is also very sensitive to the scaling of control variables. The choice of an appropriate set of control variables must be made with care. The best convergence is obtained when these variables are of the same sign and order of magnitude. Magnitudes of elastic constants which are usually used in the material's description, namely, e.g., Young's modulus, Poisson's ratio or Kirchhoff's modulus, may often be of a distinct order for typical engineering materials. Regarding the components of stiffness tensor S_{ijkl}, their magnitudes are usually of a similar order; however, they might be of different sign. While for most natural materials the signs of all components may be predicted, there are both natural and manufactured materials for which such a prediction is not so obvious—this especially regards auxetics or materials of low elastic symmetry. For this reason, the following approach was used: based on results of preliminary uniaxial tests performed with the use of standard testing techniques, approximate values of some

elastic constants should be determined to find any initial guess of the stiffness tensor components. This first approximation of the solution was assumed in the form of the isotropic fourth rank tensor, the components of which are considered to be the reference values S_{ijkl}^{ref} for those determined in subsequent iteration steps. Initial values of scaling parameters p_n which are the coordinates of vertices of initial simplex in the scale of control variables, are determined in such a way that components of the stiffness tensor are scaled randomly and independently one of another. Despite the difficulties mentioned above, the Nelder–Mead algorithm proves to be very efficient. One hundred optimization tasks for a set of one hundred profiles each performed with the use of a single core computation of a standard personal computer are completed in approximately 1 min.

3.5 Considered load step

Experimental results may in general consist of measurements of the external load for each sample at every load step. Because linear elasticity is investigated, only a single load step is considered, namely the one beyond which violation of linearity exceeds an assumed threshold.

Since the stress magnitude is unknown at the beginning of the process of material's identification, the linear range of elastic deformation is assumed to end when the linearity of the relation between recorded force and displacement is violated. The measure of non-linearity of the force–displacement relation is defined as the relative drop in sample's global stiffness $k(u) = \frac{F(u)}{u}$, where $F(u)$ is the force corresponding with the displacement u. It is assumed that within the range of linear deformation, following inequality holds true:

$$\frac{|k_0 - k_{\mathrm{end}},|}{k_0} < \epsilon, \tag{18}$$

where initial stiffness k_0 and final stiffness in the linear elastic range k_{end} are the slopes of the force–displacement curve, calculated with the use of linear regression. The threshold value was assumed $\epsilon = 0.01$.

3.6 Profiles generation

The profile which is a curve of intersection of the sample's plane and surface of the imaginary cut, which is perpendicular to the latter plane, is determined as a sigmoid logistic curve given by the following formula:

$$y(x) = \frac{A}{1 + e^{\alpha(x - x_m)}} + B, \tag{19}$$

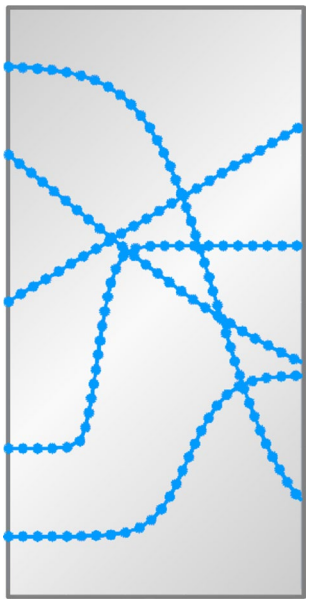

Fig. 4 Examples of generated profiles

where x and y are the coordinates (in pixels) in the gauge area. The shape of the curve depends on four parameters: parameters A and α are the vertical and horizontal scaling parameters, respectively—they determine the slope of the "step". Value $\alpha = 0$ correspond with a straight line profile, while for $\alpha \longrightarrow \infty$ the profile converges to the step function. Parameters B and x_m are responsible for vertical and horizontal shifting, respectively. Equation (19) determines only the analytical approximation of the final polygonal chain curve, the vertices of which are determined in such a way that the distance between any two such vertices is fixed and equal Δs, and will be referred to as the stress-averaging radius (Fig. 4). This modification is introduced to perform numerical integration of stress vector field along the polygonal chain curve.

3.7 Results processing

The Nelder–Mead optimization is performed multiple times for different sets of profiles as the results are sensitive to the choice of imaginary cut-surfaces. To minimize the influence of the choice of set of profiles, an average of the obtained results is considered. It is important to underline that these multiple calculations are performed with the use of just a single displacement measurement (for each considered sample), so this procedure does not require any multiple sample testing, which is the most time consuming and costly step in the process of the identification of the material's mechanical characteristics.

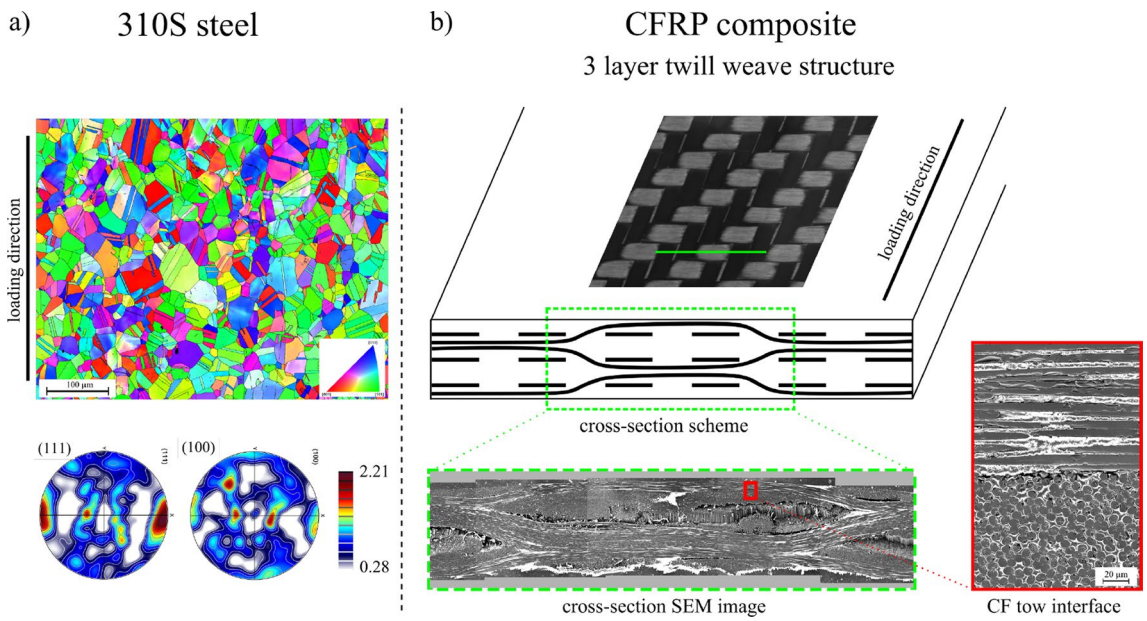

Fig. 5 Material structure of the **a** austenitic steel and **b** CFRP

4 Materials and methods

4.1 Material structure

Two materials have been examined—a 310S austenitic steel sheet and a 3-layer carbon-fiber-reinforced polymer (CFRP) (Fig. 5a). The 310S steel is a single-phase material with medium stacking fault energy (SFE) which along with the high nickel content assure the lack of deformation induced phase transformation. The microstructure studies for steel were conducted using a Zeiss Crossbeam 350 scanning electron microscope (SEM). The EBSD grain orientation map and the corresponding (111) and (100) pole figures suggest that the considered steel sheet has a small crystallographic texture. Such texture is a result of both cold rolling and applied heat treatment, i.e., annealing and subsequent water-spray quenching. For this reason, isotropy of the material is not assumed in advance and for the purpose of the identification of the constitutive relations of steel, it is described with the use of an orthotropic stiffness tensor, with one of the axes of symmetry coinciding with the rolling direction.

The tested composite was made of three layers of 2×2 twill 3k carbon fiber cloth with epoxy resin matrix. The top view of the woven structure of the composite sheet as well as the cross section are shown in Fig. 5b. Multiple approaches for the description of the composite were tested. A "step-like" or "strip-like" pattern of the strain field suggested the use of a non-homogeneous continuum for description; however, the hidden and irregular internal structure of the material made it impossible to determine the precise position, size and orientation of sub-regions exhibiting more or less uniform mechanical properties. Planes of symmetry of the microstructure of CFRP are clearly visible—this indicates that the material exhibits plane symmetry of square. Such a symmetry is not assumed in advance and in the procedure of material identification, the composite is described with the use of an orthotropic stiffness tensor. Axes of symmetry of the orthotropic structure are assumed to be aligned with the direction of fibers.

4.2 DIC analysis

Two types of samples were cut out from the 1-mm-thick sheets of the presented materials (Fig. 6b). The geometry of the standard dog-bone specimen was modified either by making an arc notch on the right-hand side (Sample A) or by introducing a hole positioned asymmetrically (Sample B). The geometry of samples was chosen to be of such a kind that the resulting strain field was inhomogeneous and that all components of the elasticity tensors could be taken into account even though only a single sub-global equilibrium condition governed the identification procedure. Another purpose of such a sample geometry is to show that the inaccuracies in the sample preparation causing possible heterogeneity in the distribution of displacement do not violate the obtained results since a full-field DIC measurement is performed and then analyzed.

The top surface of the samples was painted to obtain a suitable speckle pattern for DIC analysis. The steel samples were covered by soot with spread white dots whereas for composite samples, only small dots of white chalk were spotted. All prepared samples were deformed using a MTS

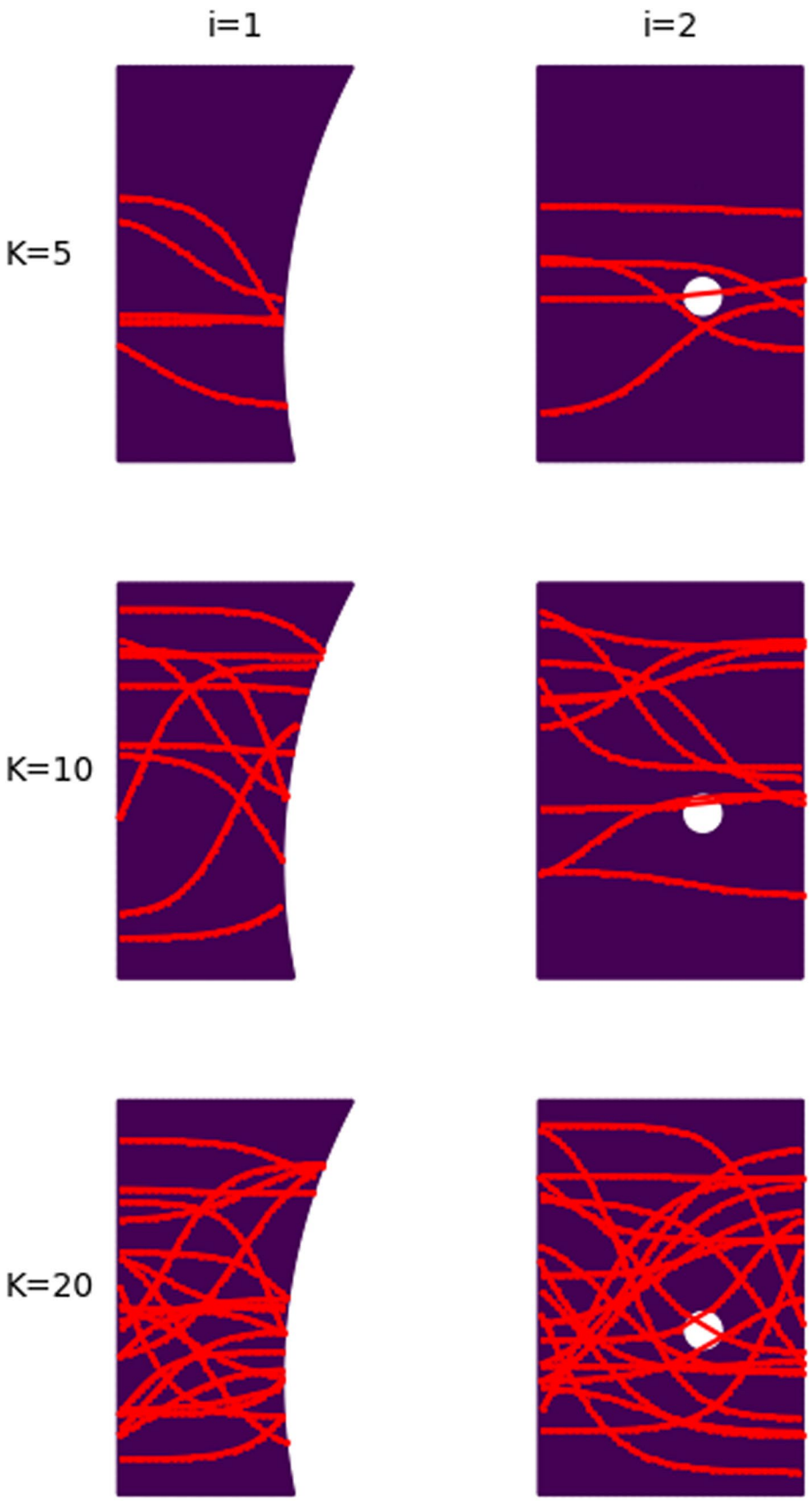

Fig. 6 Randomly generated set of profiles for i=1 (sample A) and i=2 (sample B)

858 testing machine under displacement-controlled uniaxial tension with a displacement rate of 0.015 mm/s up to the maximum displacement value of 1 mm. Due to inhomogeneous deformation of the sample the value of the strain rate was calculated as the average value of strain rate field obtained using DIC method [34]. The calculated values for all studied cases were approximately equal to 1×10^{-4} 1/s.

The experimental setup and the sample placed in the dedicated grips of the testing machine are presented in Fig. 6a (the bottom grip is fixed and the upper grip is mobile). The applied displacement rate corresponds to the quasi-static deformation process. Each of the samples was deformed beyond the elastic range to estimate the elastic limit. During all tests, the deformation of the sample surface was observed in the pco.edge 5.5 visible range camera and the sequence of gray-scale images was recorded. Camera parameters are shown in Table 1.

4.3 FEA-based verification method

A FEA-based verification was performed to check the correctness of the implementation of the algorithm, find optimal values of algorithm parameters, and estimate the error in the results obtained with the use of the SGE method. The results of the FEM analysis performed for materials of known constitutive law were used to mimic the experimental result of the DIC analysis. DIC data points were determined as being equal to nodal displacements of the FEM model. A specification algorithm based on SGE approach was then performed to find material constants and calculate the error of the method by comparing the obtained results with known values of elastic constants prescribed in the benchmark FEM model.

Generally, any deformation process can be used for verification of the proposed method; however, it was assumed that the deformation process should be possible to perform in experimental conditions. Therefore, in the first step, the finite element model of the experiment described in the previous section was created. Based on the developed numerical model, the numerical simulation of a quasi-static tensile loading process was performed to obtain the displacement field. Two classes of material were investigated—the first one exhibiting isotropic behavior and the second one exhibiting orthotropic behavior. Values of elastic constants assumed in the benchmark FEM model are given in Table 2.

For this type of material model, the stiffness tensors for the plane stress condition may be represented by matrices of the following form:

$$\begin{aligned}
\mathbf{S}^{\text{iso}} &= \frac{E}{1-\nu^2}\begin{bmatrix} 1 & \nu & 0 \\ \nu & 1 & 0 \\ 0 & 0 & 1-\nu \end{bmatrix}, \\
\mathbf{S}^{\text{ort}} &= \begin{bmatrix} \frac{E_x}{1-\nu_{xy}\nu_{yx}} & \frac{\nu_{yx}E_x}{1-\nu_{xy}\nu_{yx}} & 0 \\ \frac{\nu_{xy}E_y}{1-\nu_{xy}\nu_{yx}} & \frac{E_y}{1-\nu_{xy}\nu_{yx}} & 0 \\ 0 & 0 & 2G_{xy}, \end{bmatrix}, \\
\nu_{xy} &= \frac{E_x}{E_y}\nu_{yx},
\end{aligned} \tag{20}$$

where E stands for Young's modulus and ν is the Poisson's ratio for isotropic material, while E_x and E_y correspond to the directional Young's moduli related to the principle axes

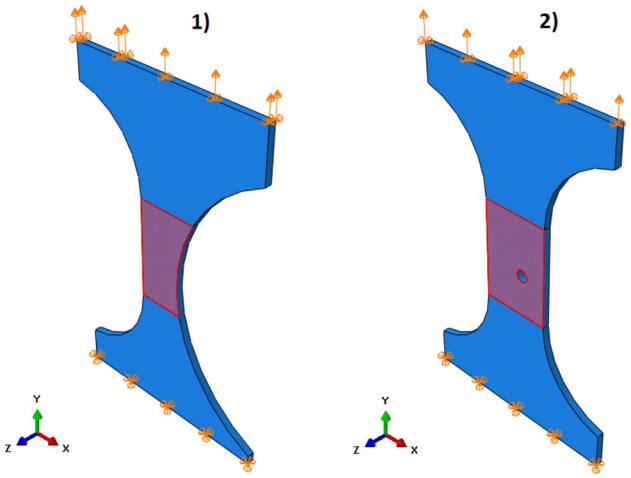

Fig. 7 Finite element models of tension tests for two kinds of sample—(1) Sample A, (2) Sample B. The marked red regions correspond to the ROI used in DIC analysis

Table 1 Parameters of the pco.edge 5.5 visible range camera used in DIC measurements

Parameters	Value
Resolution (px)	1810×2560
Recording frequency (Hz)	10
Exposure time (ms)	1.5
Pixel size (μm)	21

Table 2 Assumed material constants for isotropic and orthotropic material used in the verification procedure, similarly to those outlined in [10]

Isotropic material		Orthotropic material			
$E = 200$ GPa	$\nu = 0.3$	$E_x = 200$ GPa	$E_y = 100$ GPa	$\nu_{xy} = 0.3$	$G_{xy} = 100$ GPa

of orthotropy, ν_{xy}, ν_{yx} are the Poisson's ratios and G_{xy} is the shear modulus. In each case of the considered material, two sample configurations were considered corresponding with Sample A and Sample B used in the experiments (Fig. 7).

The set of nodes on the sample surface is defined in such a way that it mimics the ROI (region of interest in DIC analysis). Only the displacement values in this region are taken into account in calculations performed with the use of the SGE method. Additionally, the distribution of nodal reaction forces obtained from the simulation was summed to find the global reaction force which can be interpreted as a force measured by a testing machine in a real experiment.

The algorithm has been realized for both materials with the use of three data sets. The first set contained only data corresponding with Sample A, the second set concerned Sample B, while the third set contained data sets corresponding with both samples. For each of these three data sets, a specification algorithm was performed multiple times using different number of generated profiles K. The parameters of the Nelder–Mead optimization algorithm were taken as commonly chosen defaults: reflection coefficient $\alpha = 1.0$, expansion coefficient $\beta = 2.0$, contraction coefficient $\gamma = 0.5$, shrink coefficient $\delta = 0.5$. The length of a single straight segment in the polygon curve defining the profile was always assumed to be equal the average distance u between data points. Calculations have been performed for K profiles, K being the integer within the interval (1; 100). For each value of profile number, the algorithm was realized 100 times, each time for a randomly generated set of profiles. An example of such profiles for a different number of K is shown in Fig. 8.

After each computation, an error of the estimation of elastic constants was calculated—it is defined as a norm of difference between true stiffness tensor (the one assumed in the benchmark model) and of the stiffness tensor estimated with the use of SGE method. The created FE model is three-dimensional, which gives full-field 3D displacement field, while the measurement of displacements by the DIC method is only two-dimensional. The obtained error of the SGE method also takes into account this fact, i.e., satisfying the plane stress condition and verification of whether the out-of-plane deformation is negligible. The total error is then calculated as the sum of the error of the SGE method itself and the errors related to the previously mentioned effects.

5 Results and discussion

5.1 Numerical verification

In the first step, the numerical validation of the proposed SGE method was performed. A benchmark displacement field as well as the global reaction forces were determined with use of the Abaqus FE software for the a priori-assumed values of elastic constants (Table 2). Benchmark displacement fields were determined for two different sample configurations—Sample A and Sample B—the same as those used in the experiment. The calculated benchmark fields together with the force-displacement curves are shown in Fig. 9. Due to the fact that the linear elastic behavior of the material is assumed, only one calculation step in FEA is required. As it was expected for all cases,

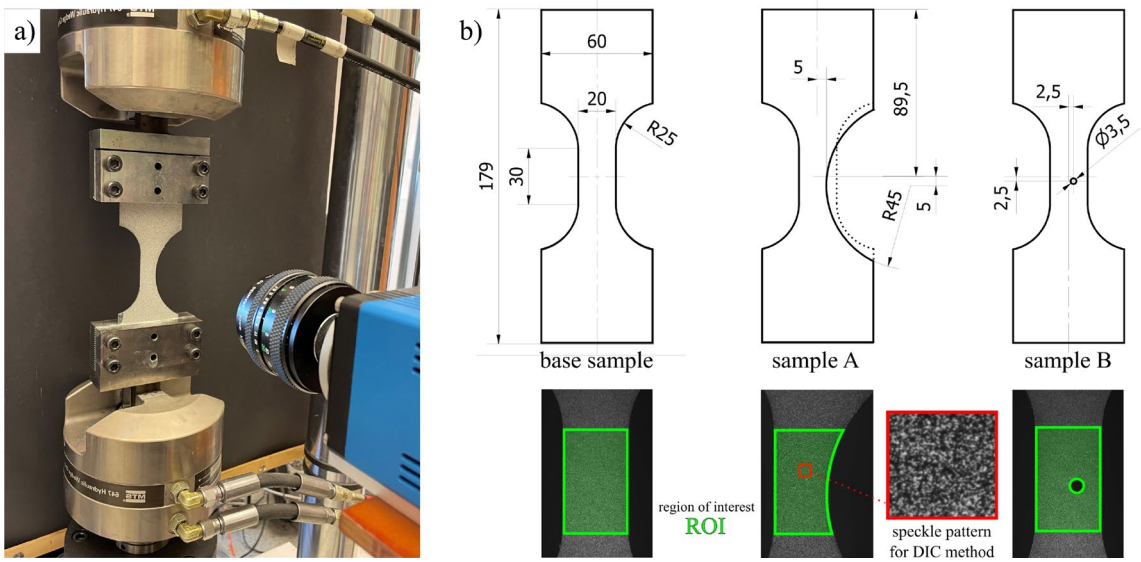

Fig. 8 **a** Experimental setup consisting of MTS testing machine and visible range camera; **b** geometry and dimensions of tested samples together with speckle pattern and region of interest (ROI) used in DIC method

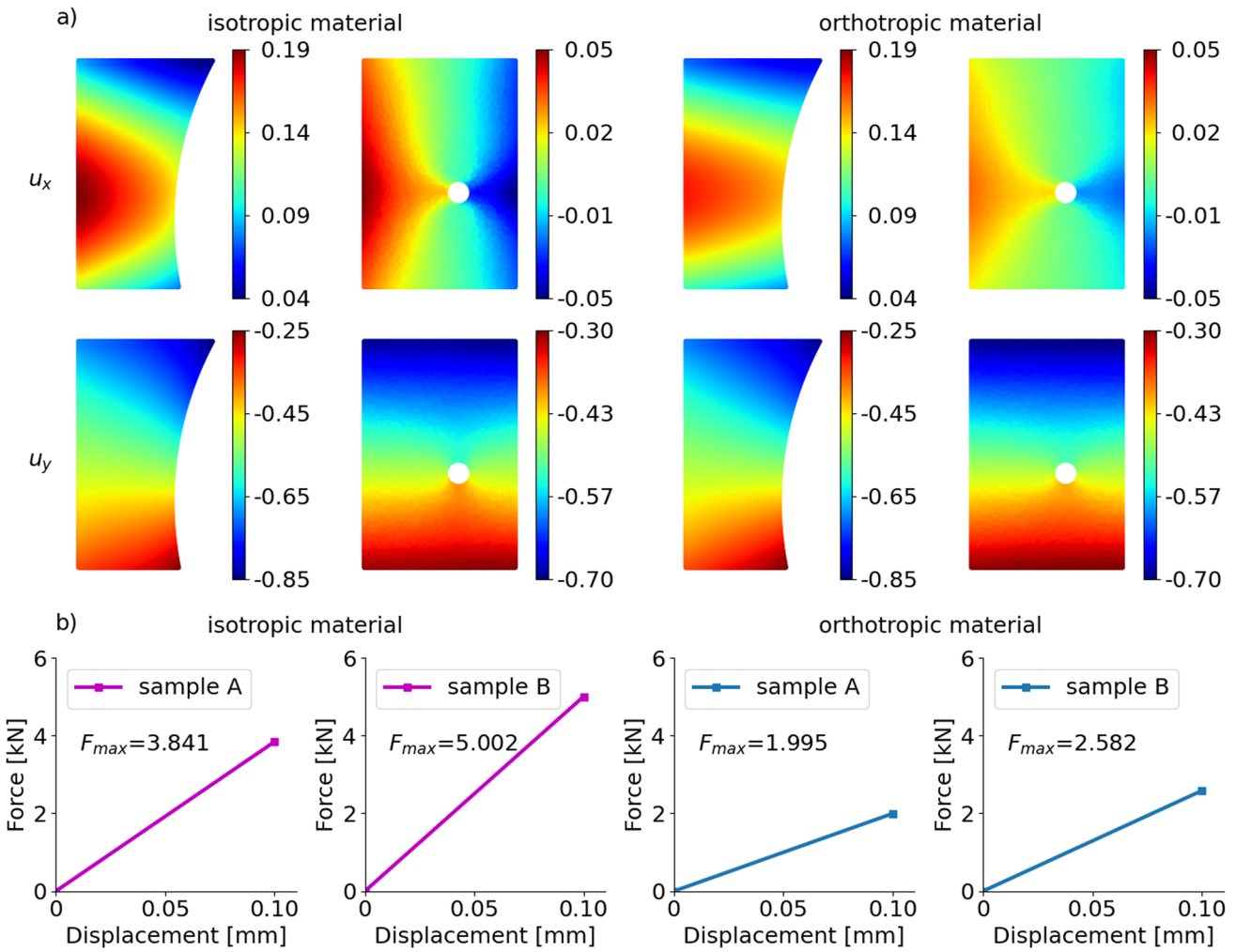

Fig. 9 **a** Displacement field for the gauge section based on the finite element calculations for isotropic and orthotropic material model; **b** global responses of the samples for a prescribed displacement $\bar{u} = 0.1\,mm$

the distributions of displacement components u_x and u_y (Fig. 9a) are heterogeneous and asymmetrical, mainly due to the specific geometry of the sample. Although the simulations are performed for two different material models, the obtained distributions are similar. By integrating the obtained stress, the vertical reaction force corresponding to the prescribed displacement $\bar{u}$ of each sample was determined (Fig. 9b).

The presented maximum force value is different for each case and it depends mainly on the assumed material constants. The results presented in Fig. 9 were used as the input data for the developed SGE method. Based on the input data, the strain distributions were calculated using first order polynomial approximation (Fig. 10). As in the case of the displacement field, the obtained distributions of strain are similar.

The mean relative errors between the known benchmark values of elastic constants and those estimated with the use of SGE method for different data sets (Sample A, Sample B, and both Samples) are presented in Tables 3 and 4 for isotropic material and for anisotropic material, respectively.

The influence of the number of profiles K on the relative error of Young's moduli E (for isotropic material) and E_x (for orthotropic material) is shown in Fig. 11.

According to the obtained results, the following general conclusions may be made:

- The mean value of the relative error obtained for one hundred algorithm runs prove to be generally insensitive to the number of profiles considered for both isotropic and orthotropic material. Typically, a spread of the results decreases gradually with the number of profiles for all considered elastic constants. This means that if the solution is obtained as the mean result of a greater number of simulations, it does not really matter if only a

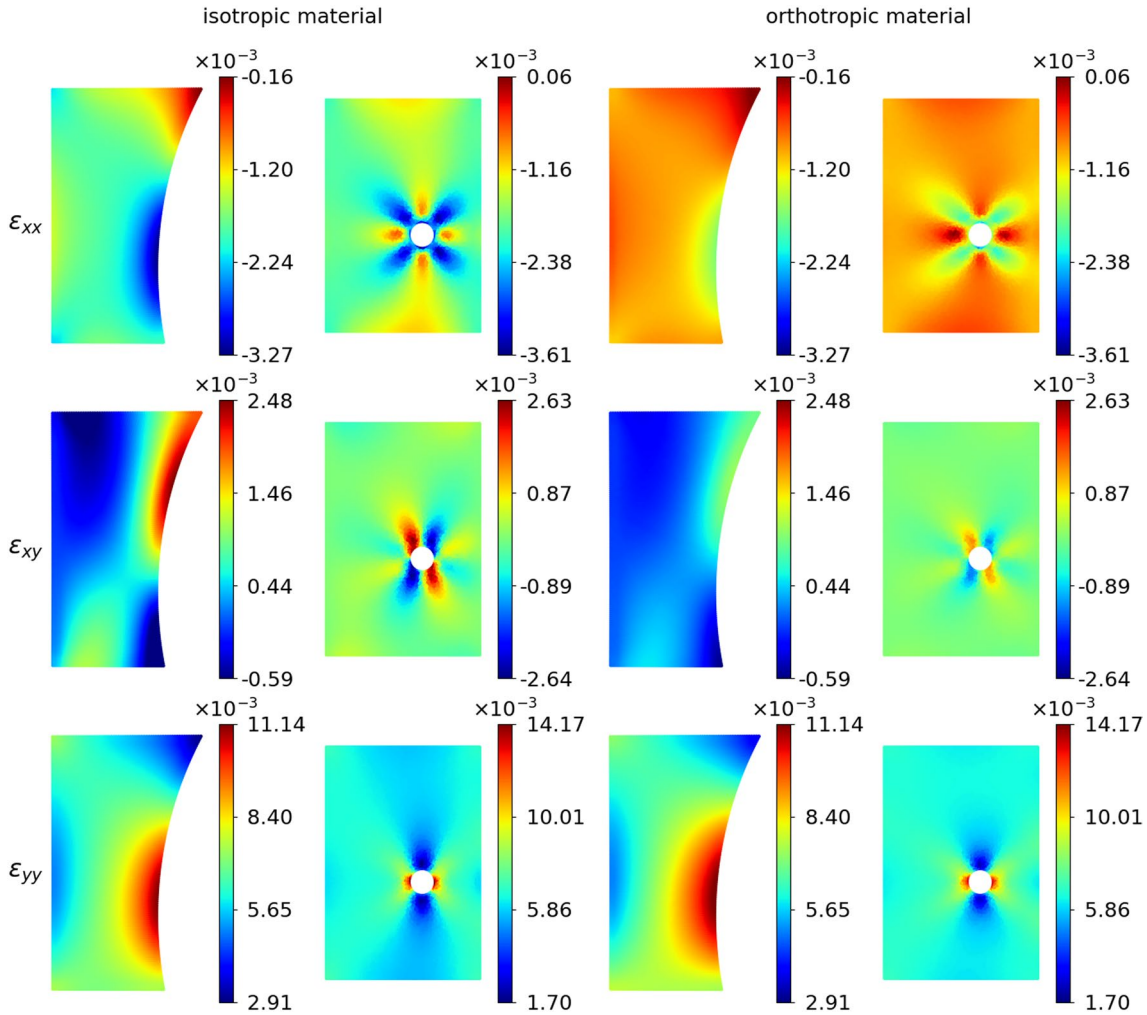

Fig. 10 Calculated strain field for the studied cases using polynomial approximation

Table 3 The mean relative error for the isotropic material model

Mean relative error (%)	*A*	*B*	*A* + *B*
E	2.70	3.56	3.49
ν	2.66	4.01	3.77

Table 4 The mean relative error for the anisotropic material model

Mean relative error (%)	*A*	*B*	*A* + *B*
E_x	3.23	4.37	3.82
E_y	13.10	16.57	17.58
ν_{xy}	10.85	9.46	9.21
G_{xy}	5.15	3.87	2.02

single profile is generated or a large profile set is considered.

- The relative error of obtained elastic constants is definitely smaller for isotropic material than for orthotropic material. This is directly related to the number of the unknowns in the optimization algorithm. For the considered material models, there are two and four unknowns for isotropy and orthotropy, respectively. The greater the number of unknowns, the lower the accuracy of their determination. The optimization algorithm is more likely to find rather a local than a global minimum for a large number of unknowns.
- A general conclusion may be made that data obtained with the use of Sample B, due to a strong localization of strain in the vicinity of a hole, enable specification of elastic constants only with greater error than if Sample A was used. It may be expected that any sample configuration resulting in high strain localization (e.g., notched

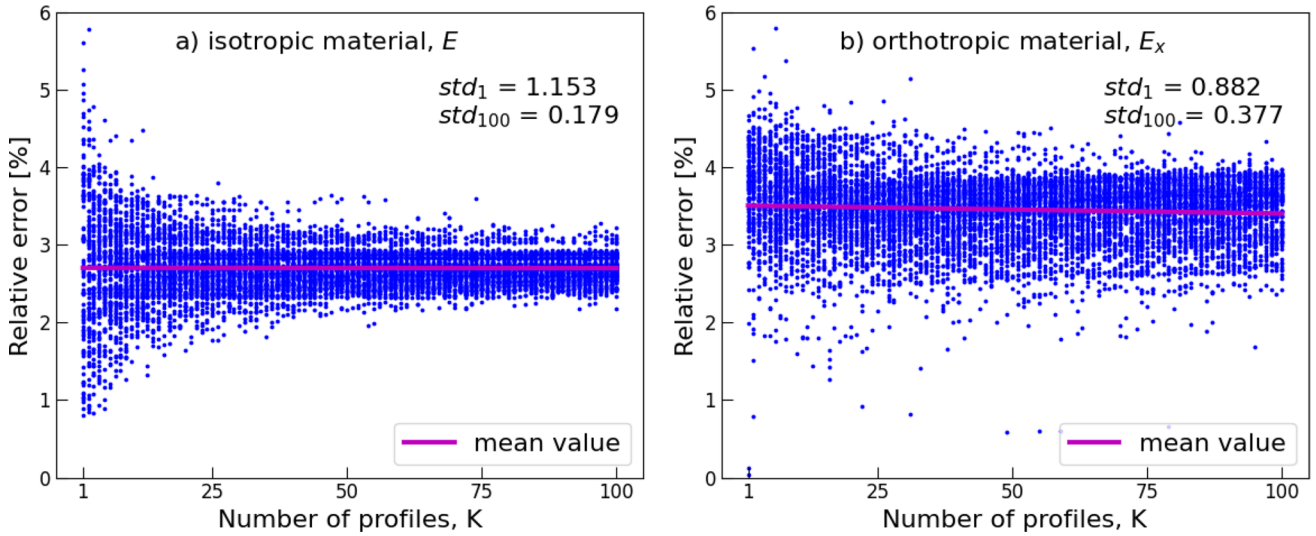

Fig. 11 Relative errors of Young's modulus as a function of number of profiles for **a** isotropic material and **b** orthotropic one. For each number of profiles one hundred algorithm runs was carried out (each point corresponds to one algorithm run). Standard deviation for one profile (std_1) and one hundred profiles (std_{100}) is shown

samples) may also provide data, for which the results of optimization is flawed with a greater degree of error.

- In the case of the data set containing displacements of both types of samples, similar dependencies may be observed as in the case of Sample B alone. One possible explanation is that the data for which the algorithm converges to a solution flawed with greater error makes a greater contribution to amplifying the value of the objective function, which is defined as a cumulative square error in satisfying the equilibrium equation. The result is that the optimal solution obtained with the use of both samples tends to produce greater error. In the view of this observation, results obtained for Sample B could be interpreted as outliers in regression performed with the use of the least squares method.

5.2 Experimental results

In a similar manner as presented in the previous section, the proposed method was used to identify material constants for the two materials described in Sect. 4. The structural characteristics of the material suggest that both considered materials can be modeled in the elastic range using orthotropic Hooke's law. The analyzed steel material should be nearly isotropic whereas the composite should exhibit the plane symmetry of a square. Following the steps of the SGE method, the displacement field obtained using the DIC method as well as the macroscopic responses of the studied cases are shown in Fig. 12.

Using Eq. (18), the limits of the linear elastic range were calculated. The vertical lines in Fig. 12b correspond to these limits. It may be noticed in Fig. 12b that distributions of displacement component u_x for composite materials exhibit a specific pattern of stripes inclined to the direction of fibres at an angle of 45°. This phenomenon depends on the internal woven structure of the composite. Similar results have been reported in the literature [35]. By calculating the displacement gradients, the strain field can be determined (Fig. 13). The specific geometry of the samples causes strain concentrations, and in the case of composite samples, a repeating pattern of high/low strain values is observed.

The elastic constants obtained using the SGE method for both steel and composite are presented in Table 5.

The results obtained for both steel and composite samples exhibit good repeatability regarding the use of different sample sets. In the case of austenitic steel for all considered sample sets, the obtained values of the E_x modulus are always slightly higher than those of the E_y. This can be related to the initial rolling texture of the tested steel, where x and y principal directions correspond to the rolling and transverse directions, respectively. In case of the composite material, the obtained E_x and E_y values are similar, as it should be expected, taking into account the microstructure of the tested CFRP material; however, the E_x values are always slightly lower than E_y.

5.3 Comparison with the results of standard tests

The material's elastic properties obtained using the proposed method were compared to those determined experimentally with the use of standard testing techniques. The uniaxial tension test was performed on standard geometry samples (see Fig. 6b) along the 0°, 45° and 90° angles from the rolling direction in steel and the first axis of orthotropy in the

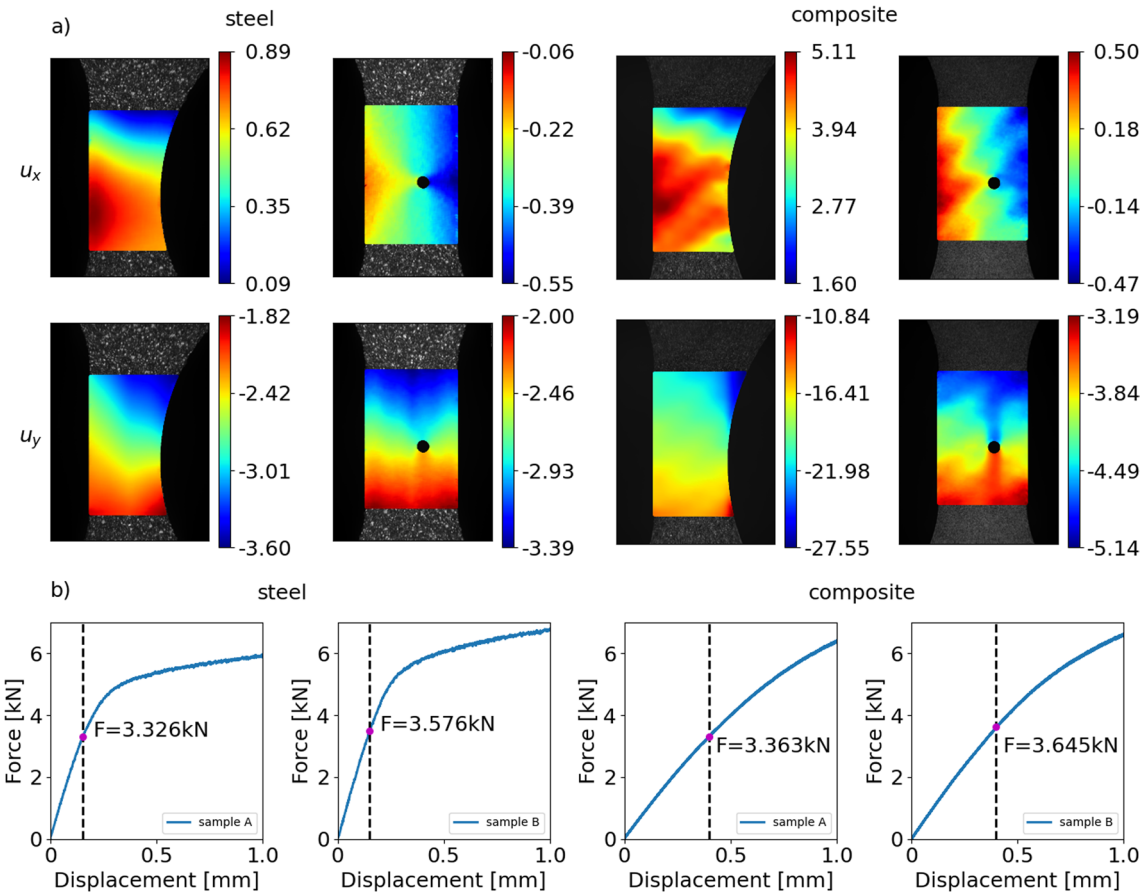

Fig. 12 **a** Displacement field obtained using DIC method; **b** the raw data from the testing machine in the form of force as a function of the applied displacement—the dashed lines correspond to the end of linear elastic range

composite. During experiments, images of the surface of the samples were acquired. To obtain the macroscopic axial strain, a virtual extensometer was marked on the reference image and the elongation between the points lying on the ends of the sample's gauge part was measured using the DIC method. The macroscopic stress was obtained based on the force measured by the testing machine and the geometry of the sample. The obtained stress–strain curves for steel and composite are presented in Fig. 14.

In the bottom row of Fig. 14, the early stage of the deformation process (up to 1% macroscopic strain) is shown. It can be seen that composite samples elongated along 0° and 90° angles fracture at less than 0.5% macroscopic strain. With regard to the 45° angle, the sample's behaviour is quite different. In this direction, the matrix deforms rather than fibres and as a result, the flow stress is much lower. The Young's modulus for both materials and all angles was determined as the slope of the linear part of the stress–strain curve (shown enlarged in the bottom row of Fig. 14). It can be seen that longitudinal stiffness of steel depends only to small extent on the orientation of load, which corresponds with the slight texture observed in the EBSD image. To make it possible to take this variation of Young's modulus into account, it is necessary to consider the material orthotropic. With regard to the composite, for the 0° and 90° angles, the slope of the elastic range is similar, which results from the composite structure. As expected, for the 45° angle, the material's response is significantly less stiff than for the other two. Additionally, the transverse strain was also determined using the DIC method and the Poisson's ratio ν_{yx} was obtained as the negative of the ratio between the transverse and axial strains. Regarding the shear modulus, its experimental determination was not considered in the paper. The experimentally obtained directional values of E and ν for steel and composite are presented in Table 6.

Based on the material constants determined using the proposed method, the directional Young's modulus may be calculated according to the following relationship:

$$E(\mathbf{n}) = \frac{1}{(\mathbf{n} \otimes \mathbf{n}) \cdot \mathbf{C} \cdot (\mathbf{n} \otimes \mathbf{n})}, \tag{21}$$

where $\mathbf{C}$ is the compliance tensor and $\mathbf{n}$ is the unit directional vector. The obtained values of $E(\mathbf{n})$ for $\mathbf{n}$ corresponding to the 0°, 45° and 90° angles were compared to the experimental

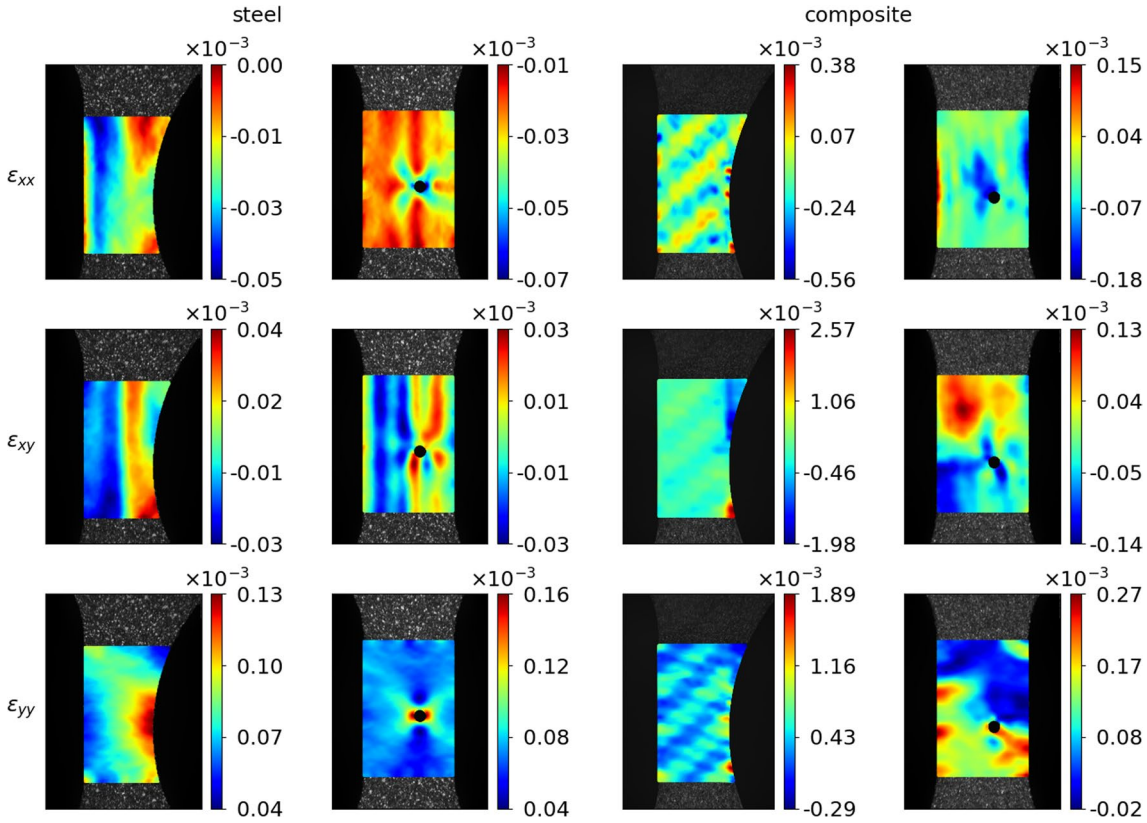

Fig. 13 Calculated strain field for the studied cases using first order polynomial approximation

Table 5 The orthotropic material parameters for both steel and CFRPcomposite identified using the SGE method

	Steel			Composite		
	A	*B*	*A* + *B*	*A*	*B*	*A* + *B*
E_x (GPa)	192.2	197.1	201.3	68.9	66.5	65.2
E_y (GPa)	172.3	174.6	174.6	72.4	73.3	70.5
ν_{xy} (–)	0.30	0.31	0.31	0.18	0.22	0.19
G_{xy} (GPa)	77.2	75.4	78.6	3.1	3.2	3.3

results. E_x and E_y are obtained directly from the SGE algorithm run, while Eq. (21) gives us:

$$E_{45} = 4\left[\frac{1}{G_{xy}} + \frac{1}{E_y} + \frac{1}{E_x} - \frac{\nu_{xy}}{E_x} - \frac{\nu_{yx}}{E_y}\right]^{-1}. \tag{22}$$

Comparison of the results of the application of the SGE method and those obtained with the use of standard testing methods is summarized in Table 7.

In the case of steel samples, the relative difference between values of Young's modulus estimated by the SGE and those determined in standard tests is less than 10% of the value obtained with the use of SGE for each data set. In the case of all data sets corresponding with composite samples, the relative difference does not exceed 6.5% regarding E_x and E_y. The discrepancy between estimates of E_{45} are far larger, reaching around 30%. The values of Poisson's ratio estimated by the SGE method differ from those determined in via the DIC analysis in standard tests with not more than 11% with regard to both materials in the case of all data sets. Better estimates are obtained for Sample B or when multiple samples are considered. In the case of composite material, the best estimates are obtained if Samples A and B are considered together.

To check whether the proposed SGE method or the standard approach gives a better estimation of the set of orthotropic elastic material constants, the force calculation procedure based on Eq. (15) was used. In the first step, the stiffness tensors $\mathbf{S}^{\text{std}}$ and $\mathbf{S}^{\text{SGE}}$ were calculated based on the material constants obtained for the standard method and SGE method, respectively. The corresponding stress fields $\boldsymbol{\sigma}^{\text{std}}$ and $\boldsymbol{\sigma}^{\text{SGE}}$ were then determined based on the

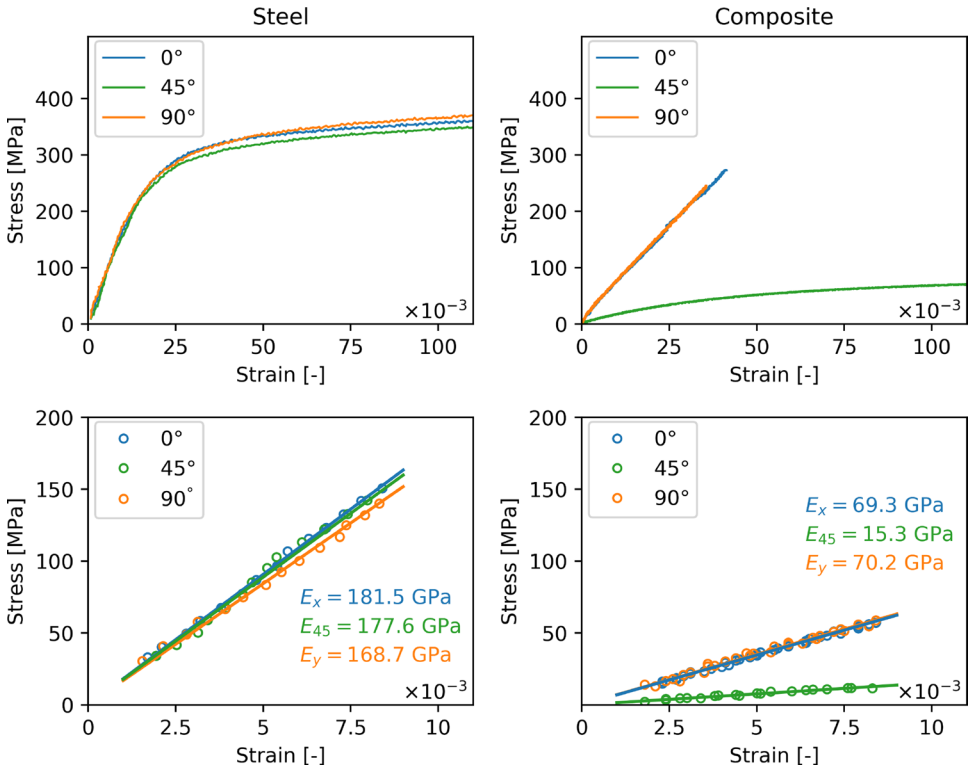

Fig. 14 The stress–strain curves obtained for steel and composite; in the lower row, the elastic ranges for both materials are shown enlarged

Table 6 The directional values of the Young's modulus and Poisson's ratio for steel and composite obtained using standard approach on the basis of uniaxial tensile test for differently oriented samples

	steel	composite
E_x (GPa)	181.5	69.3
E_{45} (GPa)	177.6	15.3
E_y (GPa)	168.7	70.2
ν_{xy} (–)	0.3	0.2
ν_{yx} (–)	0.3	0.2

Table 7 The directional values of the Young's modulus for steel and for composite obtained based on the proposed SGE method and using standard method

	Steel (data set A)		Composite (data set $A+B$)	
	SGE	Standard	SGE	Standard
E_x (GPa)	192.2	181.5	65.2	69.3
E_{45} (GPa)	190.4	177.6	12.2	15.3
E_y (GPa)	172.3	168.7	70.5	70.2

experimentally obtained strain field from the DIC method using Hooke's law. Next, the set of randomly generated profiles was created to determine the corresponding set of the internal forces. The number of profiles equal to $K = 100$ was set to take into account different local stress states of the loaded sample. The relative errors RE^{std} and RE^{SGE} between the experimentally measured force for each sample and the mean integrated internal forces obtained for the set of generated profiles obtained for both methods are presented in Table 8.

Table 8 Comparison of the mean relative errors REs of the experimentally measured macroscopic force with that calculated using Eq. (15) based on the stiffness tensor obtained using the standard and SGE methods

	Steel		Composite	
	Sample A	Sample B	Sample A	Sample B
RE^{std} (%)	6.62	5.57	15.57	14.96
RE^{SGE} (%)	3.46	4.35	13.39	13.79

The obtained results indicate that in each case, the SGE method gives a lower relative error, which suggests that the assessment of the set of elastic material constants provided by the proposed SGE method is better. This can be due to the SGE method being, in contrast to the standard method, not sensitive to the boundary conditions (accuracy in sample preparation, alignment of the sample and testing machine grips, etc.). Moreover, from the two considered sample geometries, Sample A always gives better results than Sample B, regardless of the material. It may be a result of the high local stress concentration close to the hole.

6 Summary and conclusions

The new algorithm for the identification of the elastic properties of material has been proposed. The proposed sub-global equilibrium (SGE) method allows identification of the material constants for an assumed constitutive relation by minimization of the residuum of the equilibrium equation between a known external load and internal forces estimated according to the DIC measurement. An important advantage of the proposed method over standard testing procedures is that some unavoidable imperfections in the sample preparation do not influence the final result since not only is the global force–displacement relation recorded and analyzed but the whole high-resolution full-field measurement is taken into account. However, in the case of anisotropic materials, if orientation of the axes of symmetry of the material is assumed, proper alignment of the sample is required, otherwise an additional orientation parameter needs to be included in the set of unknowns.

The proposed method is based on the most fundamental concept of static equilibrium and on the basic definition of internal forces. The only input required is the DIC measurement, contrary to VFM in the case of which it is necessary to determine appropriate kinematically admissible displacement fields. The computation in the SGE method is straightforward; with the exception of repeating independent algorithm runs to achieve better accuracy, the method does not require any iterative update procedures as is needed in the case of FEMU methods.

Numerical verification of the proposed method has been performed. FEA displacement results were used as a simulation of DIC measurement. Good agreement between SGE estimates and assumed benchmark values of elastic constants confirms the correctness of the algorithm. Performed numerical verification enables the formulation of some general conclusions. If the final estimate is computed as an average of results obtained in 100 algorithm runs, then it does not depend on the number of profiles.

Two materials have been investigated experimentally—steel exhibiting slight texture and a woven CFRP composite. Within the range of small strains, both of these were generally considered as linear elastic and orthotropic. Components of plane elasticity tensors have been determined with the use of the proposed SGE method, based on experimental results obtained for two sample types for both steel and composite. The obtained results were then compared with results obtained with the use of standard testing techniques. The error analysis has shown that the SGE method gives more accurate results even though they are obtained for one sample only, whereas the standard method requires at least three adequately oriented samples. Moreover, from two considered sample geometries, Sample A always gives better results than Sample B regardless of the materials. It is worth noting that results obtained using the proposed SGE method could be even more accurate if one optimized the sample geometry from the point of view of the desirable heterogeneity of the stress field.

According to the results of numerical verification with the use of benchmark FE models as well as the results of experiments, it may be concluded that the specification based on data referring to multiple samples should provide more reliable results (as it can be seen in the case of steel samples), but in general, they may also accumulate errors respective of each sample type (as in the case of CFRP). This may be understood in terms of the assumed method for residuum minimization, namely the least squares method. Residua calculated for multiple distinct sample types may in general be more strongly scattered than those obtained for just a single sample type. For this reason, some of the residua being minimized should be considered as outliers with regard to the whole data set. It is known that the least squares method is sensitive to this type of data variation. For this reason, it should concluded that a different minimization algorithm may provide even better results. This could be the weighted least squares method in which a scalar weight is attributed to each residuum. The objective function could then be defined as follows:

$$g(\mathbf{p}^{(n)}) = \sum_{i=1}^{I} \sum_{k=1}^{K} \left[w^{(i)} \left(F_{exp}^{(i)} - F_{\pi}^{(i,k)} \right)^2 \right], \tag{23}$$

where $w^{(i)}$ is weight respective for ith sample type. It may be estimated with the use of FE analysis of benchmark models for a given sample geometry and material type. Further improvement of the objective function g may include the use of non-dimensional quantities (similarity numbers).

The presented SGE method may be also easily generalized to make it capable of describing non-linear problems. Regarding the physical (constitutive) non-linearity, the deformation process should be divided into J steps, residuum of equilibrium equations should be calculated for each jth load step, and the sum of squares of these residua should be minimized. Regarding the geometrical non-linearity (finite strain), either of the two descriptions of non-linear elasticity—material (Lagrangian) or spatial (Eulerian)—may be used. In each of these cases, tensorial measures of stress and strain need to be chosen appropriately for the chosen description, e.g., making use of the notion of energy conjugacy. Integration of stresses along profiles may then be carried out either in the actual configuration or in the reference configuration whether either nominal stress is introduced or the well-known Nanson's formula is used.

The idea of sub-global equilibrium may also prove useful in the specification of constitutive relations which are impossible to be identified with the use of standard testing

techniques due to the complexity of constitutive law and the technical constraints imposed by the nature of the global force–displacement measurement (e.g., Mindlin's second gradient continua or Cosserat micropolar continua). Implementation of the improvements mentioned above as well as its numerical and experimental verification is within the scope of further development of the proposed SGE method.

Data availability The raw data supporting the findings of this study are available from the corresponding author, M. Nowak (nowakm@ippt.pan.pl), upon request.

Declarations

Conflict of interest The authors declare that they have no conflict of interest.

Ethical approval This article does not contain any studies with human participants or animals performed by any of the authors.

Informed consent Not applicable.

References

1. Zheng LH, Wang ZJ, Wan M, Meng B. Yield surface characterization for lightweight alloy sheets via an improved combined shear-tension experimental method. Arch Civil Mech Eng. 2022;22:96.
2. Chu TC, Ranson WF, Sutton MA. Applications of digital-image-correlation techniques to experimental mechanics. Exp Mech. 1985;25:232–244.
3. Wykes C. Use of electronic speckle pattern interferometry (ESPI) in the measurement of static and dynamic surface displacements. Opt Eng. 1982;21(3):400–406.
4. He Z, Zhang K, Lin Y, Yuan S. An accurate determination method for constitutive model of anisotropic tubular materials with DIC-based controlled biaxial tensile test. Int J Mech Sci. 2020;181:105715.
5. Martins JMP, Andrade-Campos A, Thuillier S. Comparison of inverse identification strategies for constitutive mechanical models using full-field measurements. Int J Mech Sci. 2018;145:330–345.
6. He T, Liu L, Makeev A. Uncertainty analysis in composite material properties characterization using digital image correlation and finite element model updating. Compos Struct. 2018;184:337–351.
7. Kavanagh KT, Clough RW. Finite element applications in the characterization of elastic solids. Int J Solids Struct. 1971;7(1):11–23.
8. Gajewski T, Garbowski T. Calibration of concrete parameters based on digital image correlation and inverse analysis. Arch Civil Mech Eng. 2014;14(1):170–180.
9. Gerbig D, Bower A, Savic V, Hector LG. Coupling digital image correlation and finite element analysis to determine constitutive parameters in necking tensile specimens. Int J Solids Struct. 2016;97–98:496–509.
10. Musial S, Nowak M, Maj M. Stress field determination based on digital image correlation results. Arch Civil Mech Eng. 2019;19(4):1183–1193.
11. Claire D, Hild F. A finite element formulation to identify damage fields: the equilibrium gap method. Int J Numer Meth Eng. 2004;61:189–208.
12. Ladeveze P, Leguillon D. Error estimate procedure in the finite element method and applications. SIAM J Numer Anal. 1983;20(3):485–509.
13. Roux S, Hild F. Digital image mechanical identification (DIMI). Exp Mech. 2008;48:495–508.
14. Gogu C, Yin W, Haftka R, Ifju P, Molimard J, Le Riche R, Vautrin A. Bayesian identification of elastic constants in multi-directional laminate from Moiré interferometry displacement fields. Exp Mech. 2013;53:635–648.
15. Grédiac M, Pierron F, Avril S, Toussaint E. The virtual fields method for extracting constitutive parameters from full-field measurements: a review. Strain. 2006;42(4):233–253.
16. Kim Ch, Lee MG. Finite element-based virtual fields method with pseudo-real deformation fields for identifying constitutive parameters. Int J Solids Struct. 2021;233: 111204.
17. Marek A, Davis FM, Pierron F. Sensitivity-based virtual fields for the non-linear virtual fields method. Comput Mech. 2017;60:409–431.
18. Kim Ch, Kim JH, Lee MG. A virtual fields method for identifying anisotropic elastic constants of fiber reinforced composites using a single tension test: Theory and validation. Compos B Eng. 2020;200: 108338.
19. Jiang H, Lei Z, Bai R, Wu W, Liu D, Guo Z, Yan Ch, Dong H, Li M. Identifying elasto-plastic damage coupling model of laser-welded aluminum alloy by virtual field method and digital image correlation. Opt Laser Technol. 2020;129: 106268.
20. Fu J, Yang Z, Nie X, Tang Y, Cai Y, Yin W, Qi L. A VFM-based identification method for the dynamic anisotropic plasticity of sheet metals. Int J Mech Sci. 2022;230: 107550.
21. Chalal H, Avril S, Pierron F, Meraghni F. Experimental identification of a nonlinear model for composites using the grid technique coupled to the virtual fields method. Composites A Appl Sci Manuf. 2006;37(2):315–325.
22. Avril S, Gre'diac M, Pierron F. Sensitivity of the virtual fields method to noisy data. Comput Mech. 2004;34:439–452.
23. Roux S, Hild F. Optimal procedure for the identification of constitutive parameters from experimentally measured displacement fields. Int J Solids Struct. 2020;184:14–23.
24. Avril S, Pierron F. General framework for the identification of constitutive parameters from full-field measurements in linear elasticity. Int J Solids Struct. 2007;44(14):4978–5002.
25. Mei Y, Deng J, Guo X, Goenezen S, Avril S. Introducing regularization into the virtual fields method (VFM) to identify non-homogeneous elastic property distributions. Comput Mech. 2021;67:1581–1599.
26. Voigt W. Ueber die beziehung zwischen den beiden elasticitäts-constanten isotroper körper. Ann Phys. 1889;274(12):573–587.
27. Reuss A. Berechnung der flieågrenze von mischkristallen auf grund der plastizitätsbedingung für einkristalle. Zeitschr Ang Math Mech. 1929;9(1):49–58.

28. Hollister SJ, Kikuchi N. A comparison of homogenization and standard mechanics analyses for periodic porous composites. Comput Mech. 1992;10:73–95.
29. Gan H, Orozco CE, Herakovich CT. A strain-compatible method for micromechanical analysis of multi-phase composites. Int J Solids Struct. 2000;37(37):5097–5122.
30. Kowalczyk-Gajewska K, Ostrowska-Maciejewska J. Review on the spectral decomposition of Hooke's tensor for all symmetry groups of linear elastic material. Eng Trans. 2009;57(3–4):145–183.
31. Nowak M, Maj M. Determination of coupled mechanical and thermal fields using 2d digital image correlation and infrared thermography: Numerical procedures and results. Arch Civil Mech Eng. 2018;18(2):630–644.
32. Gao F, Han L. Implementing the Nelder–Mead simplex algorithm with adaptive parameters. Comput Optim Appl. 2012;51(1):259–277.
33. Nelder JA, Mead R. A simplex method for function minimization. Comput J. 1965;7:308–313.
34. Jordan B, Grolleau V, Mohr D. Using surround dic to extract true stress-strain curve from uniaxial tension experiments. Int J Solids Struct. 2023;268: 112171.
35. Stier B, Simon JW, Reese S. Comparing experimental results to a numerical meso-scale approach for woven fiber reinforced plastics. Compos Struct. 2015;122:553–60.